

ROBUST FULL-FOV DEPTH ESTIMATION IN TELE-WIDE CAMERA SYSTEM

Kai Guo, Seongwook Song, Soonkeun Chang, Tae-ui Kim, Seungmin Han and Irina Kim

Samsung Electronics, Hwaseong-si, Korea

ABSTRACT

Tele-wide camera system with different Field of View (FoV) lenses becomes very popular in recent mobile devices. Usually it is difficult to obtain full-FoV depth based on traditional stereo-matching methods. Pure Deep Neural Network (DNN) based depth estimation methods can obtain full-FoV depth, but have low robustness for scenarios which are not covered by training dataset. In this paper, to address the above problems we propose a hierarchical hourglass network for robust full-FoV depth estimation in tele-wide camera system, which combines the robustness of traditional stereo-matching methods with the accuracy of DNN. More specifically, the proposed network comprises three major modules: single image depth prediction module infers initial depth from input color image, depth propagation module propagates traditional stereo-matching tele-FoV depth to surrounding regions, and depth combination module fuses the initial depth with the propagated depth to generate final output. Each of these modules employs an hourglass model, which is a kind of encoder-decoder structure with skip connections. Experimental results compared with state-of-the-art depth estimation methods demonstrate that our method not only produces robust and better subjective depth quality on wild test images, but also obtains better quantitative results on standard datasets.

Index Terms— Depth estimation, Hierarchical hourglass network, L1-norm scale-invariant loss function, Tele-wide camera, Full field of view.

1. INTRODUCTION

Currently tele-wide camera system with different Field of View (FoV) lenses is very popular in mobile devices, wherein each lens has different FoV, e.g. wide angle lens, tele zoom lens etc. How to obtain robust full-FoV depth for this kind of camera system becomes a challenging problem.

Usually it is difficult to obtain full-FoV depth by traditional stereo-matching methods [1, 2]. This kind of method can be formulated as a three-step pipeline including matching cost calculation [3], cost aggregation/optimization [4, 5], and disparity refinement [6, 7].

Recently Deep Neural Network (DNN) has been successfully applied to the single image depth prediction [8, 9, 10, 11, 12, 13] and tele-wide stereo depth estimation [14]. Eigen et al. [8] combined a coarse global prediction network based on the entire image with a refinement network, and proposed

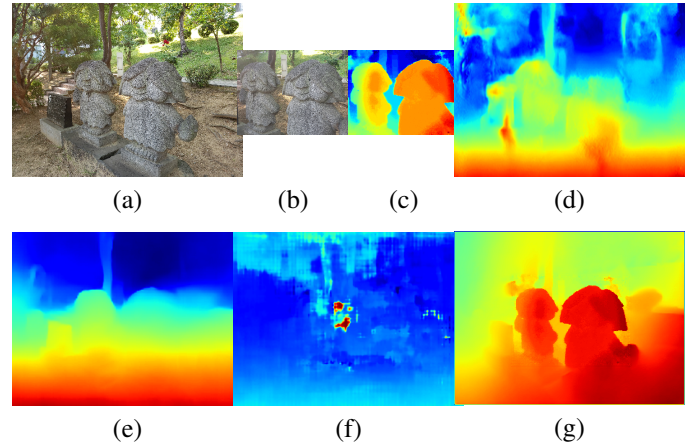


Fig. 1. Depth comparisons. (a) Wide image; (b) Tele image; (c) Traditional tele-FoV stereo-matching method: matching cost calculation/optimization [3] + post processing [7]; (d) DNN-based single image depth method in [11]; (e) DNN-based single image depth method in [13]; (f) Pure DNN-based tele-wide stereo matching method in [14]; (g) Our result.

a scale-invariant L2-norm loss function which is widely utilized in depth prediction. Laina et al. [10] developed an up-projection decoder and achieved higher accuracy. Godard et al. [11] proposed an unsupervised method to enforce disparity consistency between the left and right images, achieving similar depth quality compared with supervised methods. Li et al. [13] presented a large depth dataset called MegaDepth, which is generated from collected multi-view internet photos, the hourglass model trained on this dataset shows good results on wild test images. El-Khamy et al. [14] proposed a stereo matching neural network for tele-wide camera system so as to estimate the full-FoV depth.

Pure DNN-based methods usually have low robustness for scenarios which are not covered by training dataset [15, 16] (as shown in Fig. 1 (d, e and f)). To address the above problems, we propose a hierarchical hourglass model, which incorporates the traditional tele-FoV stereo-matching depth as input, and estimate more robust full-FoV depth on various test scenarios (as shown in Fig. 1 (g)). More specifically, the proposed network comprises three modules: single image depth prediction module that infers initial depth from input color image, depth propagation module that propagates traditional stereo-matching depth from tele-FoV to surrounding regions,

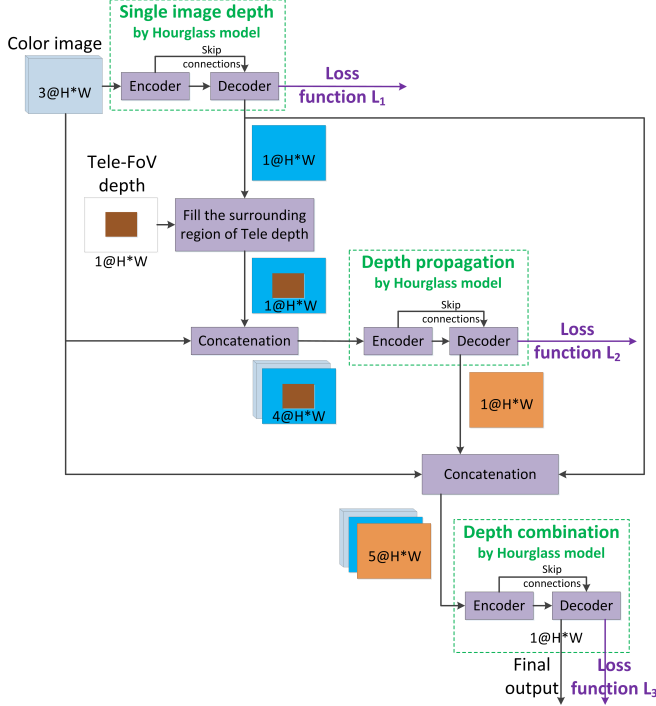


Fig. 2. Architecture of the proposed Hierarchical Hourglass network. It comprises three major modules: single image depth prediction, depth propagation and depth combination. All of these modules employ the Hourglass model [17]. The loss function of network is weighted sum of all these modules loss functions.

and depth combination module that fuses the initial depth with the propagated depth. All of them employ the hourglass model [17], which has an encoder-decoder structure with skip connections. Experiments demonstrate that our method can not only get robust and better subjective depth quality than state-of-the-art depth estimation on wild test images, but also obtain better objective results on standard datasets.

2. HIERARCHICAL HOURGLASS NETWORK

2.1. Network architecture

To estimate full-FoV depth robustly, we propose a hierarchical hourglass network which uses both wide color image and traditional tele-FoV stereo depth as input. The proposed network comprises three major modules (as shown in Fig. 2): single image depth prediction which infers initial depth from wide color image, depth propagation which propagates stereo depth from tele-FoV region to surrounding regions (wherein the stereo-matching depth is obtained by the method in [3] + post processing [7]), and depth combination which fuses the initial depth with the propagated depth to generate final output. The initial depth is also used to fill into the surrounding region of tele-FoV stereo depth, so as to make a complete full-FoV input for depth propagation module. All of these three modules employ the hourglass model [17] which has an encoder-decoder structure with skip connections.

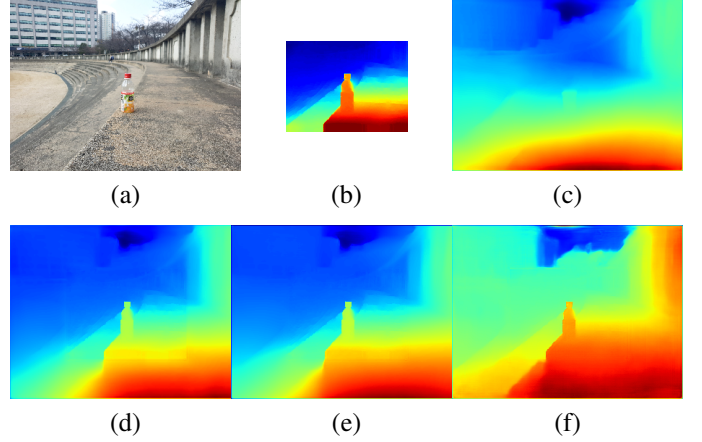


Fig. 3. Results of our network which employs the proposed L1-norm scale-invariant loss function: (c, d and e), and result of our network which employs widely-used L2-norm scale-invariant loss function [8]: (f). (a) Wide image of input; (b) Tele-FoV stereo depth of input (estimated by matching cost calculation/optimization [3] + post processing [7]); (c) Intermediate result of single image depth module; (d) Intermediate result of depth propagation module; (e) Final depth after depth combination module.

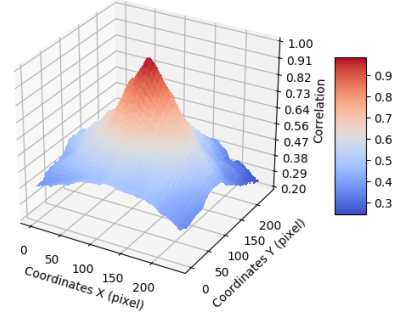


Fig. 4. Correlation between the center pixel and other pixels of depth map. This correlation is calculated based on the center 240×240 region of resized 320×240 depth maps from NYU depth V2 dataset [18].

In order to illustrate the effectiveness of each module, we compare the intermediate outputs and show them in Fig. 3 (c, d and e). The single image depth module can predict the global structure but lack of details (Fig. 3 (c)), especially for uncommon objects which are not covered by training dataset. The depth propagation module would refine the stereo depth at tele-FoV region, at the same time propagate it to surrounding regions, but has slight discontinuity artifact at tele-FoV boundary (Fig. 3 (d)). The depth combination module will fuse the initial depth with propagated depth to generate better result, and smooth out the aforementioned discontinuity artifact (Fig. 3 (e)).

2.2. Loss function

To train the whole network efficiently, we construct loss function for each module (as shown in Fig. 2), and the final loss

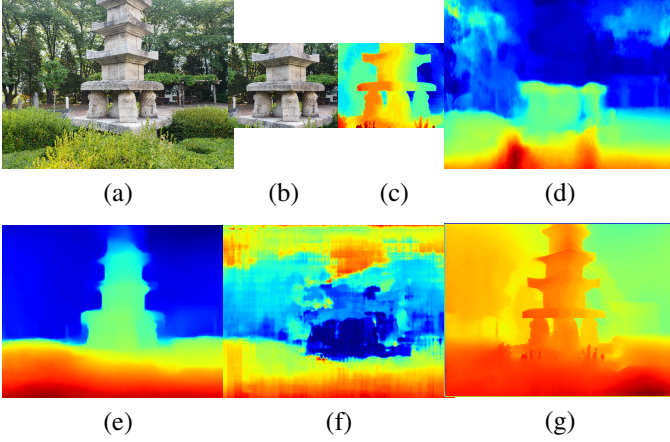


Fig. 5. Depth comparisons. (a) Wide image; (b) Tele image; (c) Traditional tele-FoV stereo-matching method: matching cost calculation/optimization [3] + post processing [7]; (d) DNN-based single image depth method in [11]; (e) DNN-based single image depth method in [13]; (f) Pure DNN-based tele-wide stereo matching method in [14]; (g) Our result.

is weighted sum of these modules loss functions.

$$L = w_1 L_1 + w_2 L_2 + w_3 L_3 \quad (1)$$

where L is the final loss, L_1 , L_2 and L_3 are the loss function of single image depth, depth propagation and depth combination modules, respectively. w_1 , w_2 and w_3 are the weights, they are set as 0.5, 0.5 and 1, respectively.

For loss function L_k , $k = 1, 2, 3$, we propose a L_1 -norm scale-invariant loss function, which regulates predicted log depth to have similar between-points relationships with ground truth. Compared with widely-used L_2 norm, L_1 norm is robust and less sensitive to outliers [19]. It is written as:

$$\begin{aligned} L_k &= \frac{1}{N^2} \sum_{i=1}^N \sum_{j=1}^N \left| \left(P_k^i - P_k^j \right) - \left(T^i - T^j \right) \right| \\ &= \frac{1}{N^2} \sum_{i=1}^N \sum_{j=1}^N \left| \left(P_k^i - T^i \right) - \left(P_k^j - T^j \right) \right| \\ &= \frac{1}{N^2} \sum_{i=1}^N \sum_{j=1}^N \left| \left(D_k^i - D_k^j \right) \right| \end{aligned} \quad (2)$$

where P_k^i and P_k^j are predicted log depth of module k at pixel position i and j , respectively. T^i and T^j are ground-truth log depth at pixel position i and j , respectively. N is the total number of pixels. D_k is the deviation between prediction P_k and ground truth T , e.g. $D_k = P_k - T$. Direct calculating the absolute difference of deviations $|D_k^i - D_k^j|$ on all possible pixels pairs is quite time consuming. To accelerate calculation, we compute absolute difference of deviations only between each pixel and its neighboring pixels, because of low correlations between a pixel and other spatially distant pixels of depth map (as shown in Fig. 4). Then the L_1 -norm scale-invariant loss function can be rewritten as

$$L_k = \frac{1}{N \times M} \sum_{i=1}^N \sum_{m=1}^M |D_k^i - D_k^{im}| \quad (3)$$

Table 1. Performance comparison on KITTI dataset. RMSE: root mean squared error; REL: mean absolute relative error; δ_i : percentage of predicted pixels where the relative error is within a threshold 1.25^i [20].

Method	Lower is better		Higher is better		
	RMSE	REL	δ_1	δ_2	δ_3
Mancini [21]	7.508	-	31.8	61.7	81.3
Eigen et al. [8]	7.156	0.190	69.2	89.9	96.7
Ma et al. [20]	6.266	0.208	59.1	90.0	96.2
Godard et al. [11]	5.927	0.148	80.3	92.2	96.4
Our method	2.440	0.05	95.2	98.3	99.3

where m is the neighboring pixels index of the pixel i , and M is the number of neighboring pixels. Absolutely the larger neighborhood would produce better results. Considering time complexity, we set neighborhood as a 17×17 window.

To justify the effectiveness of the proposed L_1 -norm scale-invariant loss function, we compare it with the result of our network which employs widely-used L_2 -norm scale-invariant loss function [8], as shown in Fig. 3 (e, f). It can be observed that the L_1 -norm loss function can generate better global structure, especially for background.

3. EXPERIMENTS

In order to validate the effectiveness and robustness of our proposed network, firstly we evaluate our method on several wild test images, which covers various different scenarios. The network is trained on MegaDepth dataset [13], where the tele-FoV depth for training is cropped from ground truth. Then we evaluate our network on two standard depth datasets: KITTI [22] and NYU Depth V2 [18], where we train our network on their training set, respectively.

3.1. Wild test images

We capture several test images at various scenarios by tele-wide camera of Galaxy S9 plus. MegaDepth [13] is employed as training dataset, which contains 200 landmarks around the world, and there are totally 100K images which have Euclidean depth data. All of the images with their depth are scaled to 240×320 , and the center 120×160 region is set as tele FoV. The training epoch number is set as 20. During test stage, the tele-FoV stereo-matching depth is obtained by the traditional stereo matching method [3] + post processing [7].

The proposed network is compared with state-of-the-art single image depth prediction methods [11, 13] and a pure DNN-based tele-wide stereo matching method [14]. All of the test codes of these methods are obtained either from their official websites or from authors. The comparison results are shown in Fig. 1 and Fig. 5. It can be observed that our method can achieve better and more robust subjective quality, especially for the foreground objects.

3.2. Standard dataset

KITTI dataset [22] contains outdoor scenes with resolution 375×1241 captured by cameras and depth sensors on a driv-

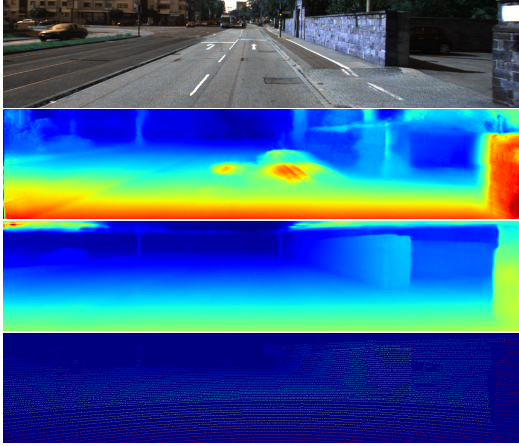


Fig. 6. Depth comparisons on KITTI test images. From top to bottom: Reference wide image, DNN method in [11], Our result, Ground truth.

Table 2. Performance comparison on NYU Depth V2 dataset.

Method	Lower is better		Higher is better		
	RMSE	REL	δ_1	δ_2	δ_3
Roy et al. [23]	0.744	0.187	-	-	-
Eigen et al. [8]	0.641	0.158	76.9	95.0	98.8
Laina et al. [10]	0.573	0.127	81.1	95.3	98.8
Ma et al. [20]	0.514	0.143	81.0	95.9	98.9
Our method	0.334	0.087	92.4	98.0	99.4

ing car. We use the 22600 training images from 28 scenes and 697 test images from another 29 scenes based on Eigen split [8]. A 256×1216 region is horizontally-random and vertically-bottom cropped from each image for training and testing, wherein the center 128×608 region of ground truth is used as tele-FoV depth for training. Our model is trained with 40 epochs. To clearly know the maximum benefit of our method regardless of stereo depth quality, we use the center 128×608 region of ground-truth depth as tele-FoV depth for test. Because all of the training and testing images are captured by the same device, we can combine the proposed L1-norm scale-invariant loss function in Equ. 3 with the common L1 norm loss function to get better results: $L_k = 0.5 \times \frac{1}{N \times M} \sum_{i=1}^N \sum_{m=1}^M |D_k^i - D_k^{im}| + \frac{1}{N} \sum_{i=1}^N |D_k^i|$, wherein D is the deviation between predicted depth and ground-truth depth.

The objective and subjective comparisons with state-of-the-art single image depth prediction methods on KITTI test set are shown in Tab. 1 and Fig. 6, respectively. Even though the training and test data are not the same across various methods, the scenes are similar because they are captured during driving and from the same sensor [20]. We can see that our model with the support of tele-FoV depth can boost RMSE, REL and δ values a lot, and also achieve better subjective quality.

The NYU Depth V2 dataset [18] consists of color images and their depth maps captured by Microsoft Kinect from 464

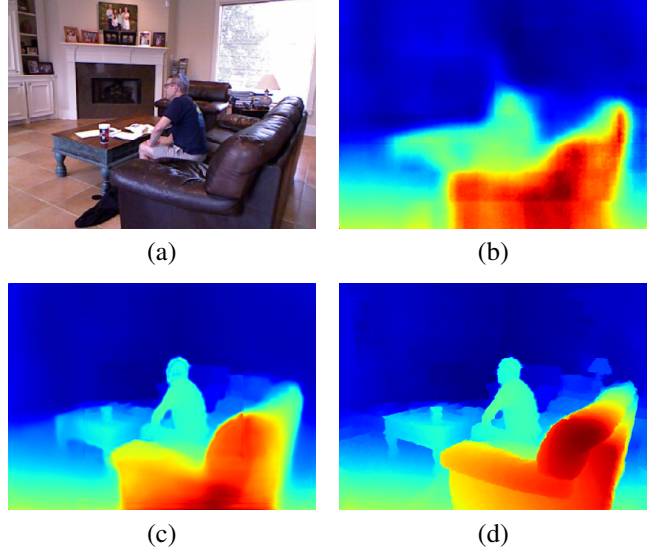


Fig. 7. Depth comparisons on NYU test images. (a) Reference image; (b) DNN method in [20]: RGB image as input; (c) Our result: RGB image + tele-FoV depth as input; (d) Ground truth.

various indoor scenes. Based on official split, we use 249 scenes for training, and 654 images [8, 10] of the rest 215 scenes for testing. All of the images with their depth maps are scaled to 224×304 , and the center 112×152 region of depth is used as tele-FoV depth for training. We use ground-truth tele-FoV depth together with color image as input for test, not only because the NYU dataset has only single image without stereo pairs, but also because we want to know the maximum benefit of our model regardless of stereo depth quality. We trained our model with 40 epochs. Because all of the training and testing images of NYU dataset are captured by the same device, we can use the combined loss function from the proposed L1-norm scale-invariant loss and the common L1 norm loss (same as KITTI dataset). The objective and subjective comparisons with state-of-the-art single image depth prediction methods are shown in Tab. 2 and Fig. 7, respectively. The comparisons demonstrate that our model can obtain better RMSE, REL, δ values as well as better subjective quality.

4. CONCLUSION

We introduced a hierarchical hourglass network for robust full-FoV depth estimation in tele-wide camera system, which combines the robustness of traditional stereo-matching methods with the accuracy of DNN methods. Experiments demonstrate its robustness and better quality in both subjective and objective evaluations. We believe this new method opens up a door for research on combining robustness of traditional signal processing into deep learning for depth estimation. In the future, we will investigate new network structure and extend our framework into other computer vision problems.

5. REFERENCES

- [1] D. Scharstein, R. Szeliski, and R. Zabih, "A taxonomy and evaluation of dense two-frame stereo correspondence algorithms," *IJCV*, vol. 47, pp. 7–42, Apr. 2002.
- [2] Y. Zhan, Y. Gu, K. Huang, C. Zhang, and K. Hu, "Accurate image-guided stereo matching with efficient matching cost and disparity refinement," *IEEE Trans. CSVT*, vol. 26, pp. 1632–1645, Aug. 2015.
- [3] D. Hernandez-Juarez, A. Chacon, A. Espinosa, D. Vazquez, J. C. Moure, and A. M. Lopez, "Embedded real-time stereo estimation via semi-global matching on the gpu," *Procedia Computer Science*, vol. 80, pp. 143–153, Dec. 2016.
- [4] H. Hirschmuller, "Stereo processing by semiglobal matching and mutual information," *IEEE Trans. PAMI*, vol. 30, pp. 328–341, Feb. 2008.
- [5] L. Zhang and S. M. Seitz, "Estimating optimal parameters for mrf stereo from a single image pair," *IEEE Trans. PAMI*, vol. 29, pp. 331–342, Jan. 2007.
- [6] J. T. Barron and B. Poole, "The fast bilateral solver," in *ECCV*, Amsterdam, Netherlands, Oct. 2016, pp. 617–632.
- [7] D. Min, S. Choi, J. Lu, B. Ham, K. Sohn, and M. N. Do, "Fast global image smoothing based on weighted least squares," *IEEE Trans. Image Processing*, vol. 23, pp. 5638–5653, Dec. 2014.
- [8] D. Eigen, C. Puhrsch, and R. Fergus, "Depth map prediction from a single image using a multi-scale deep network," in *NIPS*, Montreal, Canada, Dec. 2014, pp. 2366–2374.
- [9] J. Xie, R. Girshick, and A. Farhadi, "Deep3d: Fully automatic 2d-to-3d video conversion with deep convolutional neural networks," in *ECCV*, Amsterdam, Netherlands, Oct. 2016, pp. 842–857.
- [10] I. Laina, C. Rupprecht, V. Belagiannis, F. Tombari, and N. Navab, "Deeper depth prediction with fully convolutional residual networks," in *3DV*, Stanford, CA, USA, Oct. 2016, pp. 239–248.
- [11] C. Godard, O. M. Aodha, and G. J. Brostow, "Unsupervised monocular depth estimation with left-right consistency," in *CVPR*, Honolulu, HI, USA, July 2017, pp. 6602–6611.
- [12] H. Fu, M. Gong, C. Wang, K. Batmanghelich, and D. Tao, "Deep ordinal regression network for monocular depth estimation," in *CVPR*, Salt Lake City, UT, USA, Dec. 2018, pp. 2002–2011.
- [13] Z. Li and N. Snavely, "Megadepth: Learning single-view depth prediction from internet photos," in *CVPR*, Salt Lake City, UT, USA, Dec. 2018, pp. 2041–2050.
- [14] M. El-Khamy, H. Ren, X. Du, and J. Lee, "Tw-smnet: Multitask deep neural networks for tele-wide stereo matching," in *CVPR Workshops*, Long Beach, CA, USA, June 2019.
- [15] A. Nguyen, J. Yosinski, and J. Clune, "Deep neural networks are easily fooled: High confidence predictions for unrecognizable images," in *CVPR*, Boston, MA, USA, June 2015, pp. 427–436.
- [16] D. Su, H. Zhang, H. Chen, J. Yi, P. Chen, and Y. Gao, "Is robustness the cost of accuracy? a comprehensive study on the robustness of 18 deep image classification models," in *ECCV*, Munich, Germany, Sept. 2018, pp. 631–648.
- [17] W. Chen, Z. Fu, D. Yang, and J. Deng, "Single-image depth perception in the wild," in *NIPS*, Barcelona, Spain, Dec. 2016, pp. 730–738.
- [18] N. Silberman, P. Kohli, D. Hoiem, and R. Fergus, "Indoor segmentation and support inference from rgb-d images," in *ECCV*, Florence, Italy, Oct. 2012, pp. 746–760.
- [19] S. Gorard, "Revisiting a 90-year-old debate: the advantages of the mean deviation," *British Journal of Educational Studies*, vol. 53, pp. 417–430, Dec. 2005.
- [20] F. Ma and S. Karaman, "Sparse-to-dense: Depth prediction from sparse depth samples and a single image," in *ICRA*, Brisbane, QLD, Australia, May 2018, pp. 4796–4803.
- [21] M. Mancini, G. Costante, P. Valigi, and T. A. Ciarfuglia, "Fast robust monocular depth estimation for obstacle detection with fully convolutional networks," in *IROS*, Daejeon, South Korea, Oct. 2016, pp. 4296–4303.
- [22] A. Geiger, P. Lenz, C. Stiller, and R. Urtasun, "Vision meets robotics: The kitti dataset," *International Journal of Robotics Research*, vol. 32, pp. 1231–1237, Sept. 2013.
- [23] A. Roy and S. Todorovic, "Monocular depth estimation using neural regression forest," in *CVPR*, Las Vegas, NV, USA, June 2016, pp. 5506–5514.